Desalination and Water Treatment
www.deswater.com

doi: 10.5004/dwt.2019.24097

155 (2019) 329–340
July

Cobalt photodeposition on Fe_3O_4/TiO_2 as a novel magnetically separable visible-light-driven photocatalyst for efficient degradation of 2,4-dichlorophenol

Mona Mehdipour[a], Azadeh Ebrahimian Pirbazari[b,*], Gholam Khayati[a,*]

[a]*Technical Faculty, University of Guilan, Rasht, 416353756, Iran, emails: Khayati@guilan.ac.ir (G. Khayati), mona.mhdpr@gmail.com (M. Mehdipour)*
[b]*Faculty of Fouman, College of Engineering, University of Tehran, Fouman, 43516-66456, Iran, Tel. +981334734927; Fax: +981334737228; email: aebrahimian@ut.ac.ir (A.E. Pirbazari)*

Received 30 August 2018; Accepted 9 March 2019

ABSTRACT

In this work, we deposited different amounts of cobalt on Fe_3O_4/TiO_2 nanocomposite (FTC samples) via photodeposition method. X-ray diffraction (XRD), energy dispersive X-ray spectroscopy (EDX), field emission scanning electron microscopy (FESEM), transmission electron microscopy (TEM), diffuse reflectance spectroscopy (DRS), N_2 physisorption and the vibration sample magnetometry (VSM) were used to characterize these nanocomposites. Photocatalytic activity of the samples was examined via degradation of 2,4-dichlorophenol (2,4-DCP) under visible light. We obtained 30.42% and 57.84% degradation of 2,4-DCP after 180 min irradiation in the presence of pure TiO_2 and ternary nanocomposite containing 2.92 wt% cobalt (FTC (2.92)), respectively. The higher photocatalytic performance of FTC samples can be attributed to the high specific surface areas and the enhancing visible light absorption by cobalt. Our synthesized nanophotocatalysts can act as a novel visible light-driven and magnetically recyclable photocatalyst for environmental application.

Keywords: Cobalt; TiO_2; Fe_3O_4; Photodeposition; 2,4-dichlorophenol

1. Introduction

During the past years, photocatalytic degradation of organic contaminants in water by using semiconductor nanoparticles (NPs) has attracted intense attention [1–3]. Among various semiconductor photocatalysts, nanosized TiO_2 has attracted increasing attention because of its great chemical and thermal stability, non-toxicity and excellent degradation capacity for use in various applications including air and water purification, disinfection and waste treatment [4–6]. However, the traditional nanoscale TiO_2 applied in photocatalytic treatment of wastewater comprising organic contaminants encounters two inevitable drawbacks that limit its practical application. One disadvantage is that its high electron-hole recombination rate causes the low photocatalytic performance of TiO_2 [7,8]. To enhance its photocatalytic efficiency, a convenient and powerful approach involves the deposition of metal NPs on the surface of TiO_2 as electron acceptors, which can hinder the electron–hole pair's recombination and promote the transfer of interfacial charge in the composites [9–11]. Another disadvantage is that a separation stage is needed for removing and recovering the TiO_2 nano-catalyst from treated water as the best photocatalysis is carried out in slurry photocatalytic reactor [12,13]. To solve the reuse problem, magnetic separation using magnetic Fe_3O_4 as a carrier provides a convenient approach that can effectively enhance the recycling efficiency by using a magnet. Therefore, magnetic composites coated with TiO_2 could ease the recovery of the TiO_2 catalyst. Recently, we have various efforts to improve the photocatalytic performance corresponding to TiO_2 and deposition silver found to be an appropriate technique [14–16]. Our literatures survey showed that amongst all the existing transition metals, cobalt is one of the

* Corresponding authors.

most useful metals to increase the light response and photocatalytic performance corresponding to TiO_2. Ebrahimian et al [17] prepared cobalt doped TiO_2 nanoparticles by hydrothermal method and the synthesized samples showed a great absorption range in the visible region. Iwasaki et al [18] reported that doping of Co^{2+} into TiO_2 lattice could extended the absorption edge of TiO_2 to the visible region and improved photocatalytic performance of it under UV and visible irradiation.

The current study is aimed to study the photodeposition of different quantities of cobalt on Fe_3O_4/TiO_2 nanocomposite (FTC samples) as a new magnetic visible-light-driven photocatalyst for degrading 2,4-dichlorophenol (2,4-DCP). Based on our knowledge, this is the first report on the synthesis of Fe_3O_4/TiO_2 systems deposited by different concentrations of cobalt. Morphological and structural features of the synthesized photocatalysts were studied using different techniques including XRD, FESEM/EDX, DRS, N_2 physisorption, VSM, and TEM. The photoactivity performance of the prepared spicemens was examined by applying the photocatalytic degradation of 2,4-DCP as a model reaction. The outstanding features related with the prepared photocatalysts suggest that they can be used as a new visible light harvesting catalyst for mentioned photocatalysis applications. The ternary nanocomposites showed a better performance for photocatalytic degradation of 2,4-DCP compared with pure TiO_2.

2. Experimental

2.1. Materials

$FeCl_3{\cdot}6H_2O$ (Merck No. 103943) and $FeSO_4{\cdot}7H_2O$ (Merck No. 103965) were utilized for synthesizing Fe_3O_4 NPs. Tetraisopropyl orthotitanate (TIP, Merck No. 8.21895), anhydrous ethanol, ammonia, and High-purity 2,4-DCP, 98% (Merck No. 803774) for photocatalytic tests as probe molecules were purchased from Merck company (Germany). Cobalt (II) chloride hexahydrate ($CoCl_2.6H_2O$) (Merck, No.102539) was obtained from Merck Company. All the substances were of analytic grade and used with no further purification. All aqueous solutions were synthesized with deionized water.

2.2. Preparation of Fe_3O_4 NPs

Fe_3O_4 NPs were synthesized by chemical precipitation technique based on the process mentioned in [19]. In this procedure, Fe_3O_4 was precipitated under an inert atmosphere (nitrogen 99.999%) and alkaline conditions.

2.3. Synthesis of Fe_3O_4/TiO_2 nanocomposite

In this section, 0.1 g Fe_3O_4 NPs was synthesized based on the process mentioned in section 2.2., 4 mL tetraisopropyl orthotitanate (TIP) was combined with 70 mL anhydrous ethanol and ultrasonicated (ELMA-Germany, E60H, ultrasound bath) for 1 h to form the solution A. In order to prepare solution B, 3 mL acetic acid was diluted by 90 mL deionized water. Solution B was mixed with solution A drop wise at 50°C through the mechanical stirring. Then, the solution was agitated for 30 min. Finally, after cooling to room temperature, the solid product from the suspension was separated by employing a magnet, washed several times with ethanol and water, and dried at temperature of 60°C for 12 h. The annealing of resultant powder was carried out at temperature of 300°C for 1 h to synthesize Fe_3O_4/TiO_2 nanocomposite. From now on, this specimen will be presented as FT. Furthermore, pure TiO_2 was prepared through similar method to control the experiments.

2.4. Photodeposition of cobalt on Fe_3O_4/TiO_2 nanocomposite

We carried out the photodeposition of cobalt on Fe_3O_4/TiO_2 nanocomposite according to mentioned method in references [15,20]. In this step, 0.3 g Fe_3O_4/TiO_2 powder and different amounts of $CoCl_2.6H_2O$ (3.6, 7.2 and 14.4 mg) were added to 16 mL deionized water under magnetic stirring. Then, 4 mL methanol was inserted into the supernatant. The obtained solution was irradiated by a UV-Vis light lamp (400W Kr lamp, Osram, Germany, with 90% illumination power in the UV-A region and about 10% in the UV-B region) for 2 h. After that, the precipitate was filtered and fully washed with deionized water and ethanol three times to remove the residual impurities. From now on, these specimens will be presented as FTC (a), where (a) represents the amount of cobalt achieved by EDX analysis.

2.5. Photodeposition of cobalt on TiO_2

In this step, 0.3 g TiO_2 powder and 7.2 mg of $CoCl_2.6H_2O$ were added into 16 mL deionized water under magnetic stirring. Then, 4 mL methanol was inserted into the obtained suspension, followed by irradiating with a UV-vis light lamp (400W Kr lamp, Osram, Germany, with 90% illumination power in the UV-A region and about 10% in the UV-B region) for 2 h. Next, the suspension was separated and carefully washed with deionized water and ethanol three times to eliminate the residual impurity. From now on, these samples will be shown as TC.

2.6. Characterization

Using an X-ray detractor (Siemens, D5000, Germany), the XRD patterns for crystalinity investigation were obtained by means of CuK_α radiation as the X-ray source. The diffractograms were determined within the 2θ range from 20° to 80°. The morphology corresponding to the achieved specimens were studied using scanning electron microscope (SEM, Vegall-Tescan Company, Czech Republic) having an energy dispersive X-ray (EDX) for chemical composition analysis. The UV-visible diffuse reflectance spectra (DRS) corresponding to the specimens were obtained for band gap energy calculation by means of an Ava Spec-2048TEC spectrometer. The microstructure and morphology corresponding to the synthesized specimens were studied using a transmission electron microscopy (TEM) device (Philips CM30 300 kV). The nitrogen physisorption assessments were done by a Quantachrome Autosorb-1-MP (`). The BET areas were measured using static physisorption of nitrogen at temperature of –196°C followed by out-gassing at temperature of 200°C until reaching a pressure smaller than 5 mbar. VSM system is manufactured by Meghnatis Daghighe Kavir (MDK) Company, Kashan, Iran used for magnetic properties measurement.

2.7. Photocatalytic degradation of 2,4-DCP

2,4-DCP was chosen as a model of organic pollutant to examine the photocatalytic performance corresponding to the prepared specimens. A500W, OSRAM Halogen lamp (ECO) (350 to 800 nm, with a 400 nm cut-off filter) was used for visible light tests. In every photocatalytic degradation test, the baker comprising photocatalyst and 100 mL 2,4-DCP aqueous solution (40 mg L^{-1}) was first agitated in the dark for 10 min for adsorption/desorption equilibrium (Fig. 1), followed by turning the lamp for 180 min. At certain times, 2 mL of solution were withdrawn and filtered to eliminate the photocatalyst and analyzed using Rayleigh UV-2601 UV/VIS spectrophotometer (λ_{max} = 227 nm).

3. Result and discussion

3.1. X-ray diffraction analysis

Figs. 2 and 3 present the XRD patterns corresponding to the prepared specimens. In XRD pattern corresponding to Fe_3O_4 NPs (Fig. 2(a)), the characteristic diffractions were observed at 2θ = 30.2°, 35.6°, 43.5°, 54.3°, 57.4°, and 63.1° that are related to the reflection of cubic spinel structure corresponding to the Fe_3O_4. These findings are in agreement with those observed using JCPDS card number 19-0629 [21], proposing that pure phase of Fe_3O_4 and well-resolved diffraction bands show the crystalline structure of Fe_3O_4 NPs. In XRD pattern corresponding to pure TiO_2 (Fig. 2(b)), the strong diffractions at 2θ = 25.3°, 37.7°, 48.0°, 53.8°, 55.0°, and 62.6° proved formation of pure anatase phase [22]. In XRD pattern corresponding to Fe_3O_4/TiO_2 (FT) sample (Fig. 2(c)), the diffractions became relatively weaker than those of the pure TiO_2 and Fe_3O_4 (Fig. 2(b)), but in a good accordance with the XRD pattern of TiO_2. Also, we detected some weak diffractions of Fe_3O_4 NPs in Fig. 2(b), which may indicate that Fe_3O_4 is coated by TiO_2 and confirm that the spicemen comprises Fe_3O_4 and TiO_2. Figs. 3(a) to (d) showed the XRD patterns corresponding to FTC and TC samples. We detected the key diffractions for anatase phase of TiO_2 in these samples but did not find the key diffractions for metallic cobalt. Comparing with the pure TiO_2, the peak intensity of FTC and TC samples was found decline, signifying that the crystallinity degree was lowered because of the strong interaction between the cobalt with the TiO_2 support [23]. We didn't observe the diffractions at 2θ = 38.55°and 74.12° were contributed to Co_3O_4 based on the PDF#42-1467 [24] and the diffraction at 2θ = 38.61° corresponded to Co_2O_3 spinel structures based on the PDF # 02-0770. Because of the low level, great distribution, and small crystalline sizes corresponding to cobalt particles, we did not find the key diffractions corresponding to metallic cobalt in XRD patterns of the ternary FTC nanocomposites and TC sample. The average TiO_2 crystal dimension at 2θ = 25.3° was computed for each specimen using Scherrer equation [25]:

$$D = K\lambda/\beta \cos\theta \quad (1)$$

where D represents the mean crystallite size in nm, λ refers to the X-ray wavelength (1.54056 Å), β is the diffraction full width at half maximum (FWHM) in radian, K represents a coefficient (0.89),and θ refers to the diffraction angle. The TiO_2 crystal dimension in all the prepared nanocomposites is within the nanosized range (Table 1). The lattice parameters (a = b ≠ c) relating with tetragonal crystalline structure were

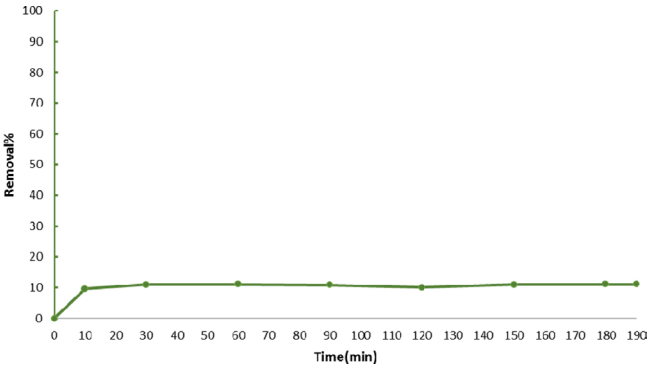

Fig. 1. Time of adsorption/desorption equilibrium for 10 mg of FTC (2.92) in 100 mL of 2,4-DCP (40 mg L^{-1}).

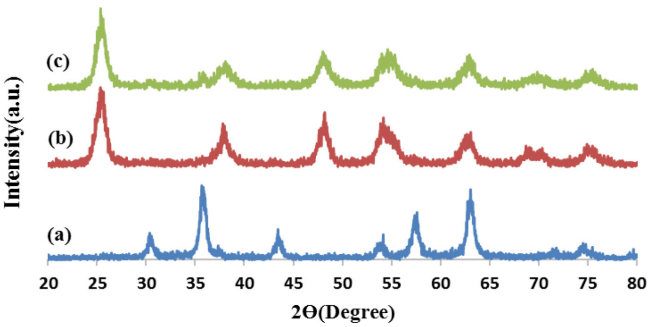

Fig. 2. XRD patterns of (a) Fe_3O_4, (b) TiO_2, (c) FT.

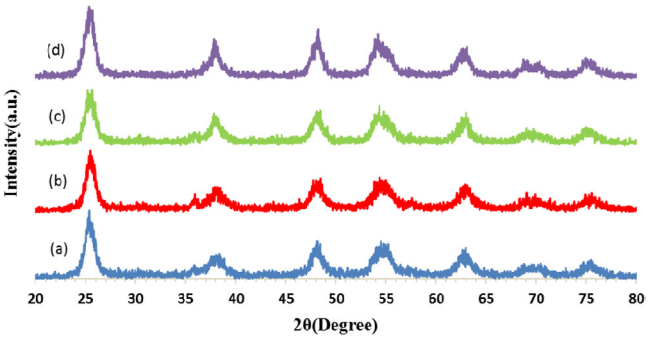

Fig. 3. XRD patterns of (a) FTC (1.26), (b) FTC (2.05), (c) FTC (2.92), (d) TC.

Table1
Phase, crystal size and lattice parameters of the prepared samples

Sample	Phase	Crystal size (nm)	a = b (Å)	c (Å)	Cell volume (Å3)
T	Anatase	7.930	3.783	9.429	134.939
TC	Anatase	7.485	3.778	9.622	136.730
FT	Anatase	8.885	3.798	9.200	132.740
FTC (1.26)	Anatase	7.688	3.780	9.490	135.596
FTC (2.05)	Anatase	8.414	3.760	9.440	133.450
FTC (2.92)	Anatase	7.294	3.750	9.750	137.109

achieved for (101) crystal plane corresponding to anatase phase using Eq. (2):

$$1/d^2 = (h^2 + k^2)/a^2 + l^2/c^2 \quad (2)$$

Considering the interplanar spacing (d_{hkl}), the distance between adjacent planes in the set Miller indexes (hkl) can be determined using the Bragg Law:

$$d_{hkl} = \lambda/2 \sin\theta \quad (3)$$

The volume of cell (tetragonal one) was computed as:

$$V = a^2c \quad (4)$$

where a and c represent considered lattice parameters. Table 1 indicates the lattice parameters corresponding to the synthesized specimens. The achieved values for the lattice parameters of TiO_2 in the synthesized specimens were in a good accordance with the TiO_2 anatase phase (JCPDS, 78-2486) [16]. The diffractions and lattice parameters for TiO_2 were not affected, approving no cobalt atoms enter into the TiO_2 framework and loading of cobalt atoms on the surface of TiO_2 NPs as well as no variation of the crystal structure of TiO_2.

3.2. UV-Vis absorption spectra

The solid-state UV-Visible spectra (Fig. 4(A)) were obtained for all the specimens. There is a wide intense absorption about 400 nm in the DR spectrum corresponding to pure TiO_2, because of the charge-transfer from the valence band resulted by 2p orbitals of the oxide anions to the conduction band created by 3d t_{2g} orbitals of the Ti^{4+} cations [26]. The diffuse reflectance spectra of the samples containing cobalt, showed extra broad absorption peak between 500 to 750 nm. The origin of the absorption peak is attributed to charge-transfer interaction of Co_2+/Ti^{4+} [27]. Moreover, this may be the cause of higher photoactivity of these samples under the visible light compared with pure TiO_2. We also measured the band gap energy for the prepared specimens from the DR spectra based on Eq. (5) [28].

$$[F(R)\,h\upsilon]^{0.5} = A\,(h\upsilon - E_g) \quad (5)$$

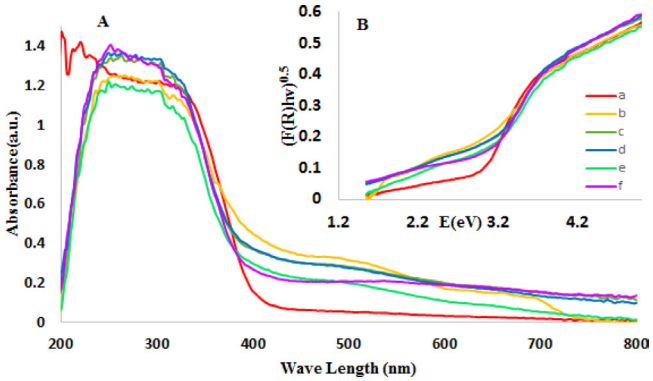

Fig. 4.(A) Diffuse reflectance spectra and (B) Kubelka-Munk plots for the band gap energy calculation of (a) T, (b) TC, (c) FT, (d) FTC (1.26), (e) FTC (2.05) and (f) FTC (2.92).

where A is the constant, $F(R)$ is the function of Kubelka-Munk, and E_{bg} (eV) is the band gap. Table 2 shows the E_{bg} data corresponding to specimens. The band gap of FTC samples reduced a little compared with TiO_2 (Table 2). Cobalt NPs loading on the surface of TiO_2 influence considerably on the optical features of TiO_2. Evidently, the FTC photoresponse of the nanocomposite is significantly shifted toward the visible light region owing to the presence of cobalt NPs.

The effect of metal presence on TiO_2 band gap reduction can be attributed to:

1. The charge-transfer transitions between the metal ion d electrons and the TiO_2 conduction or valence band.
2. The formation of contamination levels in the band gap of TiO_2; if these states locate near the band edges, they can overlap band states, narrowing its band gap [29].
3. The creation of allowed energy states in the TiO_2 band gap, as a result of the existence of segregated M_xO_y clusters on its surface [30] that can induce photoactive transitions in visible light, due to an excitation of an electron from this energy level into the TiO_2 conduction band. Consequently, the existence of metal species can affect TiO_2 photoactivity altering the electron–hole pair recombination rate. Fig. 4(B) shows the Kubelka-Munk curves for the synthesized samples.

3.3. FESEM/EDX and TEM analyzes

Figs. 5 and 6 show the FESEM images corresponding to the prepared specimens at two magnifications. The FESEM images corresponding to FTC samples indicate that TiO_2 coated the surface of Fe_3O_4 NPs. To confirm successful decoration of Fe_3O_4/TiO_2 nanocomposites with cobalt, the specimens were studied using electron mapping image analysis (Fig. 7). The images of the same samples were obtained for Ti, O, Fe, and Co. For FTC samples, Ti had a broader distribution compared with Fe, showing that Fe is set in the interior section of the nanocomposites. In comparison, Ti and Co lie on the outer layer of the Fe_3O_4 NPs. These outcomes show that cobalt NPs are well spread on the Fe_3O_4/TiO_2 nanocomposite surface. The EDX patterns of the samples (Fig. 8) display two peaks about 0.2 and 4.5 keV. The strong peak is related to the bulk TiO_2 and the less strong one is related to the surface TiO_2. Fig. 8 shows the peaks corresponding to cobalt at 0.6, 6.9 and 7.5 keV. The less strong peak is allocated to cobalt in the TiO_2 lattices [26,31]. The elemental chemical analysis of the prepared samples is shown in Table 3. These outcomes showed the existence of cobalt atoms in the specimens, while no diffraction corresponding to cobalt was found in the

Table 2
Band gap energy of the prepared samples

Sample	Eg (eV)
TiO_2	2.90
FT	2.80
TC	2.56
FTC (1.26)	2.78
FTC (2.05)	2.79
FTC (2.92)	2.81

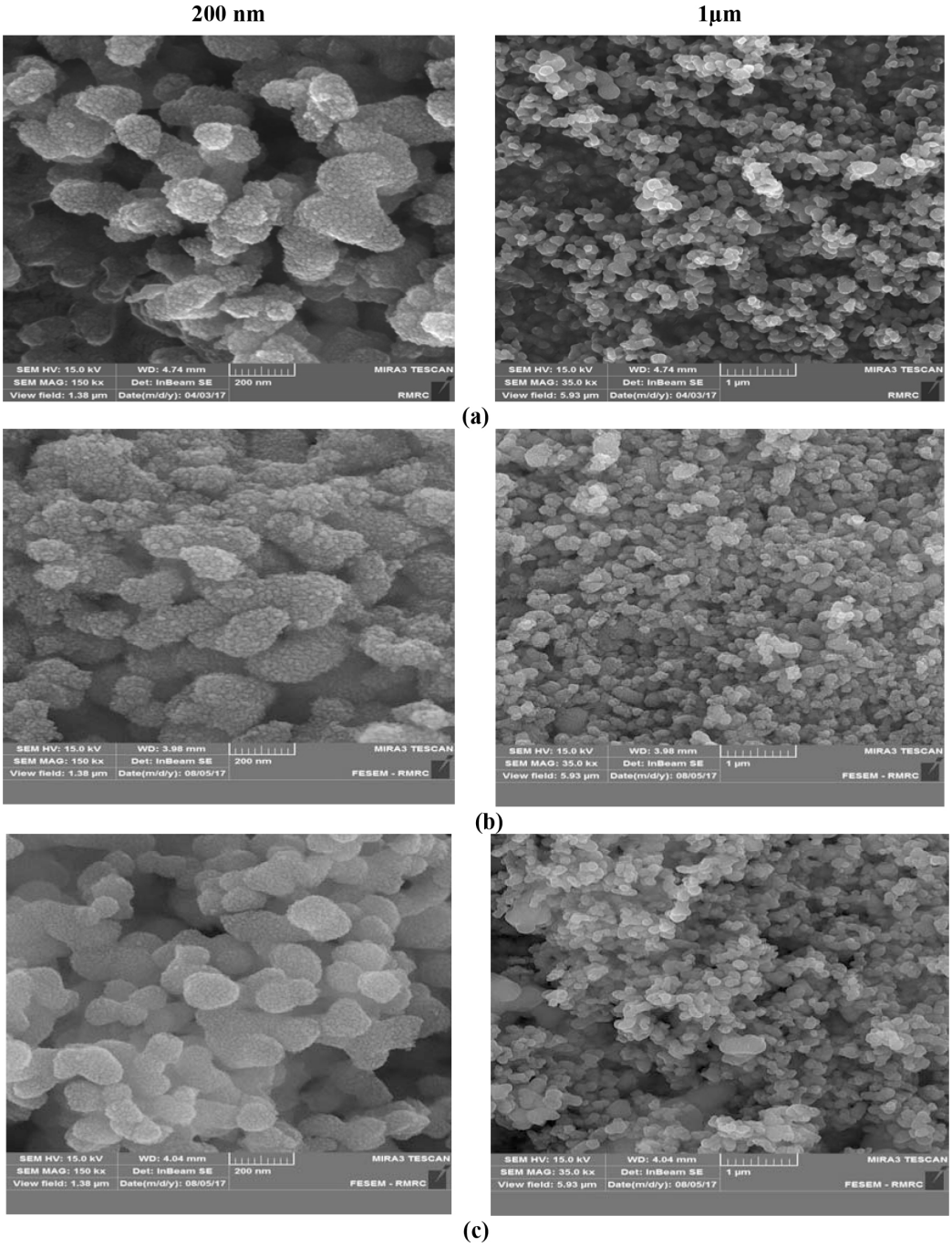

Fig. 5. FESEM images of (a) T, (b) TC, (c) FT.

XRD patterns. Fig. 9 depicts the TEM image of FTC (2.92) (photocatalyst with the maximum photoactivity among the ternary nanocomposites) at different magnifications. The dark grains of magnetite NPs (Fe_3O_4) are fully surrounded via gray TiO_2 layer that contains TiO_2 NPs and cobalt nanoparticles according to elemental mapping results.

3.4. N_2 physisorption analysis

The results of N_2 adsorption-desorption isotherms are shown in Fig. 10. The sorption isotherms for all synthesized specimens relate with the type IV isotherm based on the classification of IUPAC [32]. Table 4 shows textural and structural parameters corresponding to the prepared specimens. Specific surface areas were computed based on BET. Pore volumes and mean pore diameter were extracted from the desorption branch based on the model of BJH. The S_{BET} of the FT sample is more than the pure TiO_2 but the mean pore diameter of FT sample is smaller than pure TiO_2. This observation may prove that the nanolayer of TiO_2 covered the Fe_3O_4 NPs. The BET surface area corresponding to the cobalt containing samples is more than that of the initial

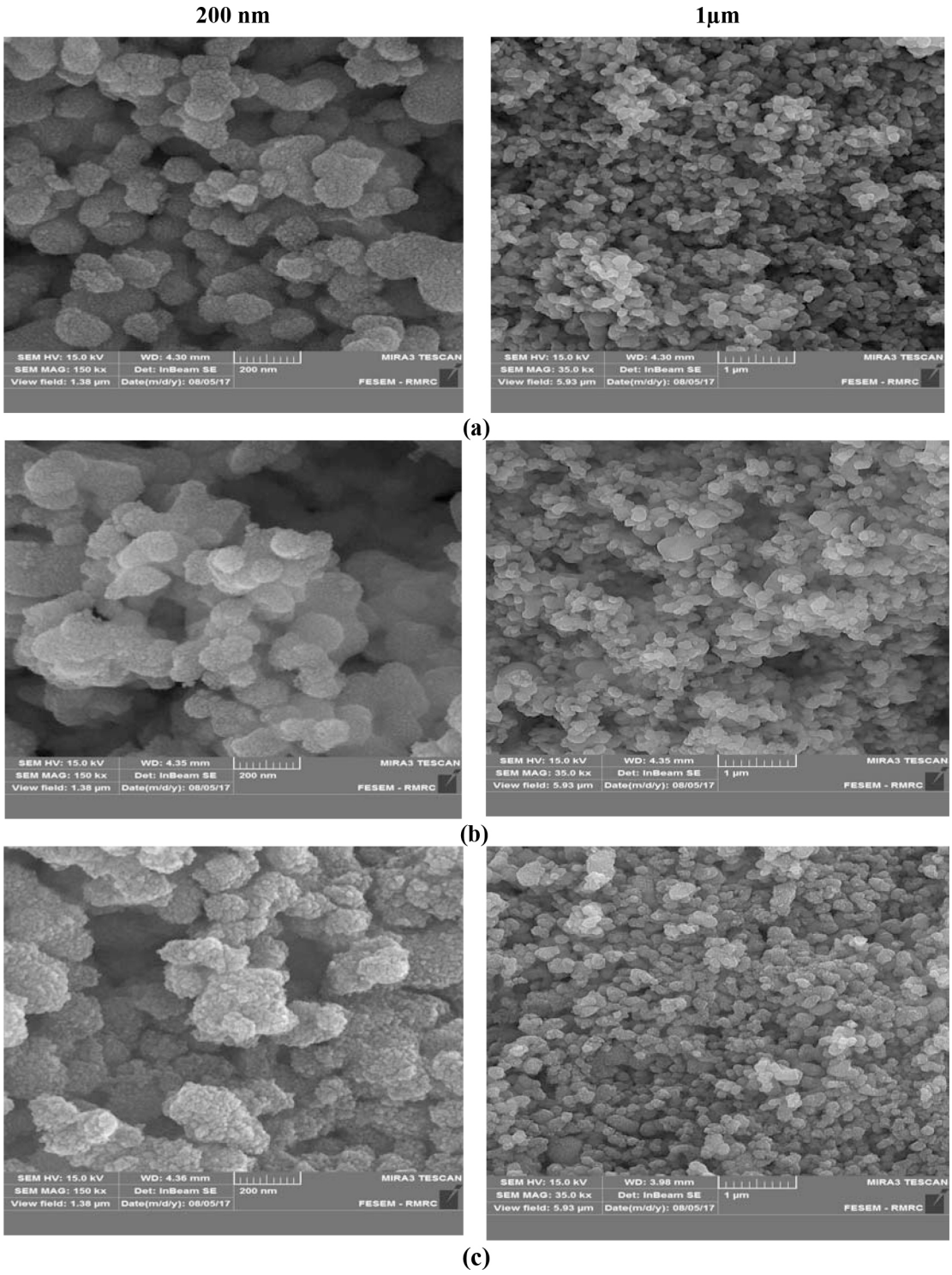

Fig. 6. FESEM images of (a) FTC (1.26), (b) FTC (2.05), (c) FTC (2.92).

TiO_2, indicating the deposition of cobalt NPs on the surface of TiO_2.

3.5. Magnetic properties of the samples

The saturation magnetization (Ms) corresponding to the specimens were determined using the magnetic reaction corresponding to the magnetic nanocomposites to an external field. Based on Fig. 11, the photocatalysts are superparamagnetic at ambient temperature [33]. It must be noted that the Ms value corresponding to the Fe_3O_4 NPs (62.41 emu g^{-1}) is considerably more than that of FT (2.20 emu g^{-1}), FTC (1.26) (1.63 emu g^{-1}), FTC (2.05) (1.98 emu g^{-1}) and FTC (2.92)(2.13 emu g^{-1}) specimens, which is owning to the coating of Fe_3O_4

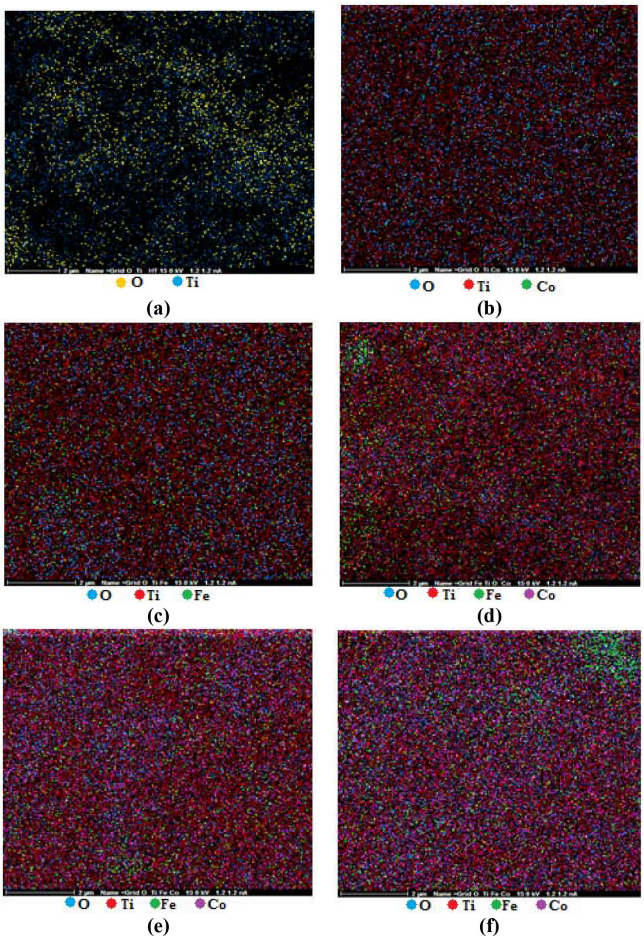

Fig. 7. Elemental mapping of (a) T, (b) TC, (c) FT, (d) FTC (1.26), (e) FTC (2.05) and (f) FTC (2.92).

NPs with an anatase TiO_2 layer. The slight reduction in Ms value of the FTC specimens comparing with that of the FT sample (Fig. 11) can be described by the small enhance in mass and dimension due to the adherence of cobalt NPs to the magnetic composites surface. Additionally, no important change was observed in the coercivity. Such excellent magnetic features suggest a strong magnetic responsivity on the samples, enabling them to be recycled easily from solution through an external magnetic force. Also, easy, fast separation and redispersion of the FTC specimens can be observed (Fig. 11).

3.6. Photocatalytic degradation of 2,4-DCP under visible light

To study the photocatalytic behavior corresponding to the obtained specimens for removal of contaminants from wastewater, photocatalytic degradation of 2,4-DCP was chosen as a model reaction. Fig. 12 shows the photocatalytic degradation of 2,4-DCP under visible light. Under visible light, the ternary photocatalyst with 2.92 wt% cobalt, FTC (2.92) specimen presented the maximum activity for photocatalytic degradation of 2,4-DCP and we achieved 57.84% degradation after 180 min irradiation. The two main parameters affecting the performance of photocatalyst are surface area and absorption capacity of the light. Outcomes of the DRS analysis (Fig. 4) indicate that the obtained specimens have diverse light absorption capacities and these capacities enhance with increasing the concentration of cobalt in visible region. Consequently, enhancing the concentration of cobalt has two opposite effects on the photocatalytic performance of the FTC samples; enhancing light absorption capacity and reducing surface area (Table. 4). The photocatalytic performance is affected by which one of these is the main factor. Also, it can be seen from Table 4 and Fig. 11, FT sample has larger surface area and shows better degradation performance more than

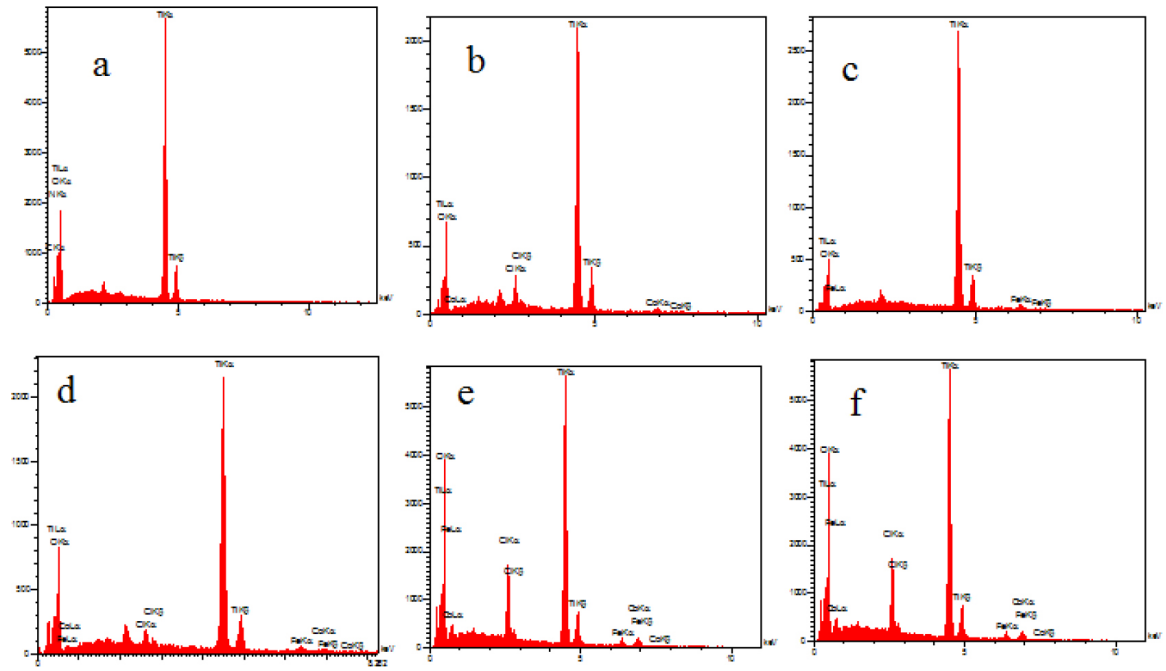

Fig. 8. EDX spectra of (a) T, (b) TC, (c) FT, (d) FTC (1.26), (e) FTC (2.05) and (f) FTC (2.92).

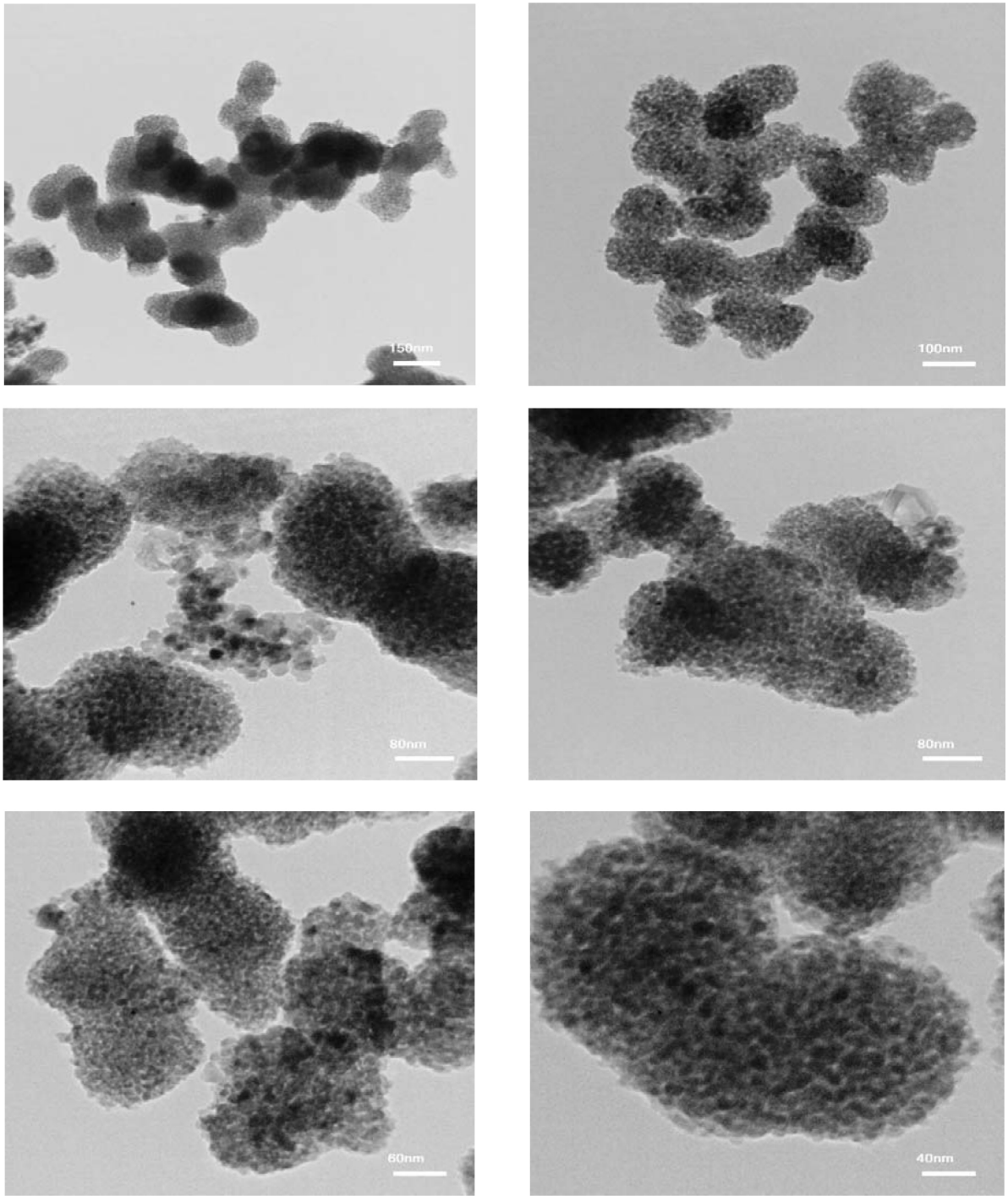

Fig. 9. TEM image of FTC(2.92) nanocomposite at various magnifications.

ternary ones. But our main purpose of this research was the investigation of photocatalytic performance of FT nanocomposite after cobalt deposition. Our obtained results indicated that the cobalt deposition didn't enhance photocatalytic activity of FT sample.

Fig. 13 shows the mechanism proposed in the current study for the formation of FTC sample and 2,4-DCP photocatalytic degradation over FTC sample. High-energy electrons were formed on TiO_2 in ternary nanocomposites under visible light. These formed electrons were moved and excited from TiO_2 to cobalt NPs and the formed holes remained on the valance band of TiO_2 and oxidize the organic target. The oxygen molecules adsorbed on the surface of photocatalyst trapped the electron from the cobalt and thus a number of active species including $OH^{\bullet}$ and $O_2^{\bullet-}$ radicals were produced. These species attacked 2,4-DCP molecules and decomposed them. Because of the heterojunctions generation, many defects exist in TiO_2 that reduce

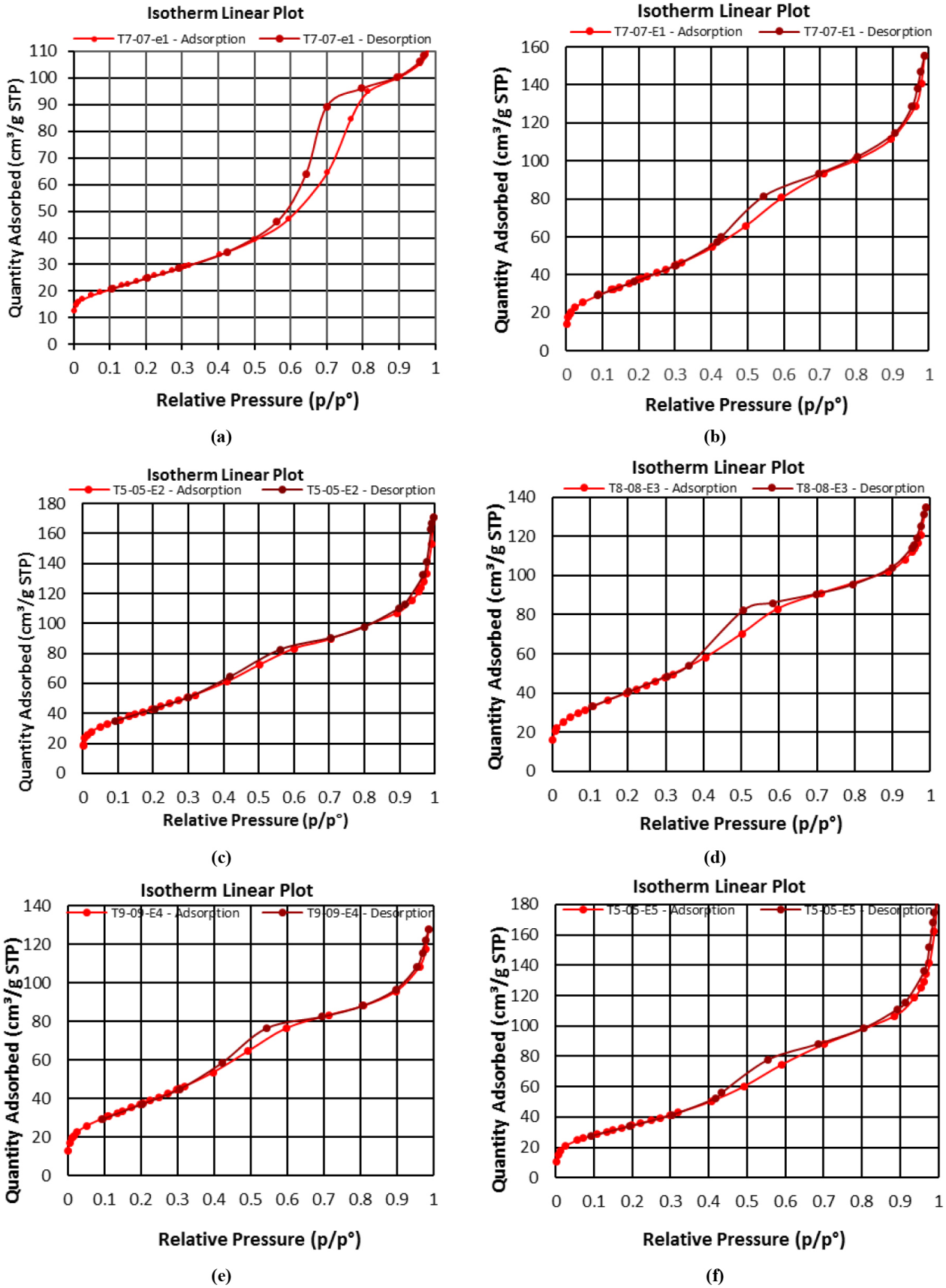

Fig. 10. N_2 adsorption–desorption isotherms for (a) T, (b) TC, (c) FT, (d) FTC (1.26), (e) FTC (2.05) and (f) FTC (2.92).

Table 3
Elemental chemical analysis of the prepared samples

Sample	Cl (wt%)	Fe (wt%)	O (wt%)	Ti (wt%)	Co (wt%)
T	–	–	52.41	47.59	–
FT	–	2.09	39.80	58.11	–
TC	2.74	–	48.34	47.46	1.46
FTC (1.26)	1.40	1.69	50.60	45.04	1.26
FTC (2.05)	2.35	1.41	50.32	43.86	2.05
FTC (2.92)	5.66	1.95	55.64	33.82	2.92

Table 4
Textural and structural parameters of the prepared samples

Sample	S_{BET} ($m^2\ g^{-1}$)	Average pore diameter (nm)	Pore volume ($cm^3\ g^{-1}$)
T	91.01	7.16	0.17
Fe_3O_4	86.55	11.37	0.26
TC	144.86	5.44	0.25
FT	159.43	4.83	0.25
FTC (1.26)	153.47	4.48	0.22
FTC (2.05)	142.43	4.65	0.21
FTC (2.92)	131.31	6.10	0.29

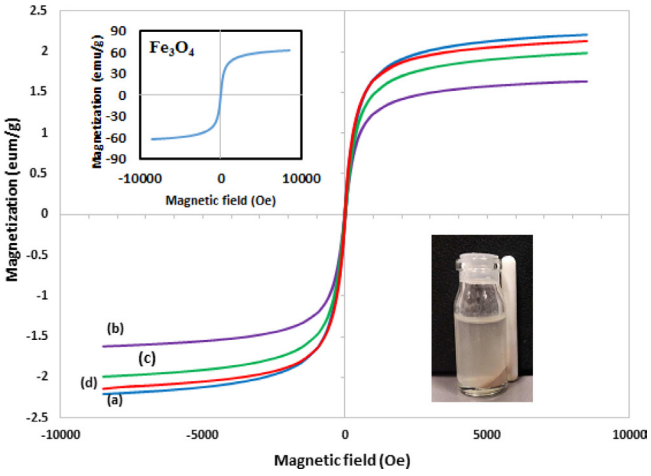

Fig. 11. Comparison of hysteresis curves of (a) FT, (b) FTC (1.26), (c) FTC (2.05) and (d) FTC (2.92).

the energy corresponding to conduction band for TiO_2 [34] of the ternary nanocomposite. FTC samples can offer a larger surface area (Table 4), contributing to the improved photocatalytic function induced by its improved photon absorption [35].

3.7. Effect of photocatalyst amount

At low photocatalyst loading the elimination of the organic compound 2,4-DCP increased linearly with the catalyst loading. However, existence of the extra photocatalyst in the aqueous solutions could cause a shielding effect in penetration of light [36]. In this regard, the effect of the photocatalyst dose in suspension was investigated for an optimal condition (Fig. 14). The optimal phtocatalyst amount is 10 mg/100 mL for degradation of 2,4-DCP.

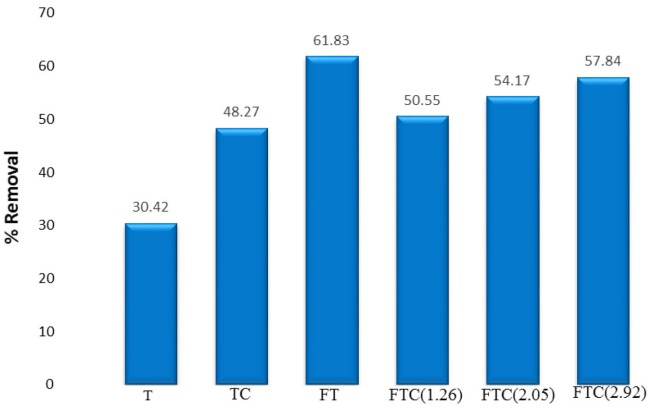

Fig. 12. Photocatalytic degradation of 2,4-DCP in the presence of the prepared samples under visible light.(Initial concentration of 2,4-DCP – 40 mg L^{-1}; volume – 100 mL; catalyst dosage – 10 mg).

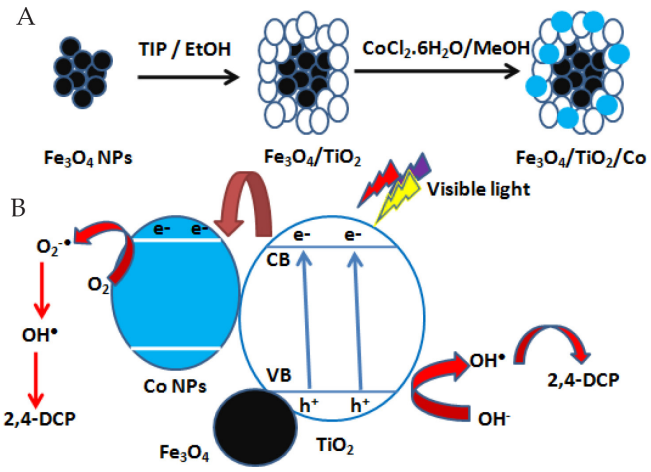

Fig. 13. Our proposed mechanism for (a) formation of FTC sample and (b) photocatalytic degradation of 2,4-DCP over FTC photocatalyst under visible light.

3.8. Recyclability of FTC (2.92)

The stability and recyclability of catalyst is crucial to the running cost of wastewater treatment and business economic benefits, thus the stability of FTC (2.92) photocatalyst was evaluated for three consecutive photocatalytic cycles (Fig. 15). No significant decrease was observed in the photocatalytic performance of FTC (2.92) nanocomposite because of the presence of magnetic Fe_3O_4 for removal of 2,4-DCP. The results represent that FTC could be a recyclable and promising photocatalyst for the application.

4. Conclusion

Generally, visible light-driven and magnetically recyclable ternary Fe_3O_4/TiO_2/Co photocatalysts comprising diverse concentrations of cobalt (FTC samples) were synthesized

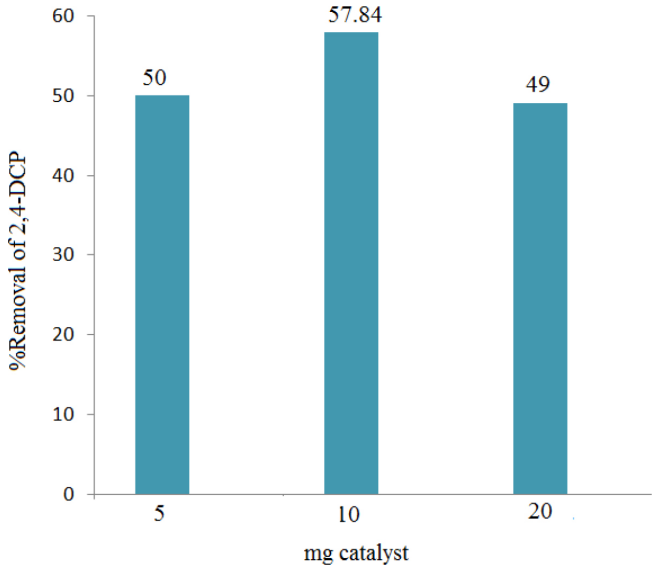

Fig. 14. Effect of photocatalyst amount on degradation of 100 mL of 2,4- DCP (40 mg L^{-1}) after 180 min irradiation under visible light.

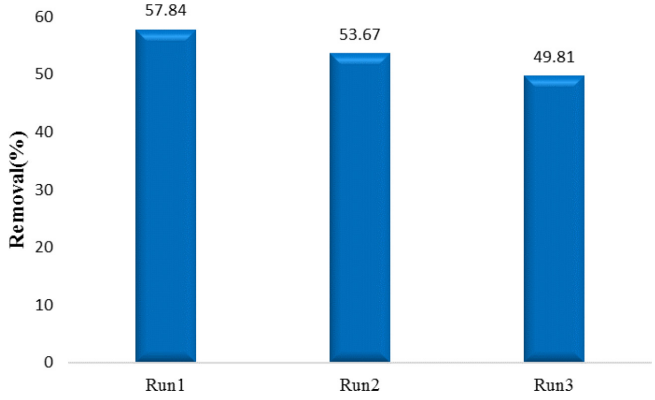

Fig. 15. Recyclability of the FTC (2.92) for photocatalytic degradation of 2,4-DCP under 180 min visible light after three successive cycles (photocatalyst dose: 10 mg/100 mL; [2,4-DCP]: 40 mg L^{-1}).

by the simple sol-gel and photodeposition method. The characterization of prepared photocatalysts was performed through various techniques including XRD, DRS, TEM, VSM, N_2– physisorption, and FESEM/EDX. The ternary sample containing 2.92 wt% cobalt exhibited the maximum photocatalytic performance for degrading 2,4-DCP among ternary nanocomposites. We obtained 57.84% and 30.42% degradation for 2,4-DCP in the existence of FTC (2.92) and TiO_2, respectively. The excellent photocatalytic performance of ternary nanocomposites can be related to both the high specific surface areas of them and the enhancing visible light absorption by cobalt.

Acknowledgment

The authors wish to acknowledge the financial support of the University of Guilan and University of Tehran for supporting of this research.

References

[1] J.S. Lee, J. Jang, Hetero-structured semiconductor nanomaterials for photocatalytic applications, J. Ind. Eng. Chem., 20 (2014) 363–371.
[2] P.A.K. Reddya, P.V.L. Reddy, E. Kwon, K. H Kim, T. Akter, S. Kalagara, Recent advances in photocatalytic treatment of pollutants in aqueous media, Environ. Int., 91 (2016) 94–103.
[3] J. Chen, F. Qiu, W. Xu, S. Cao, H. Zhu, Recent progress in enhancing photocatalytic efficiency of TiO_2-based materials, Appl. Catal., A., 495 (2015) 131–140.
[4] K. Kabra, R. Chaudhary, R.L. Sawhney, Treatment of hazardous organic and inorganic compounds through aqueous-phase photocatalysis: a review, Ind. Eng. Chem. Res., 43 (2004) 7683–7696.
[5] X.B. Chen, S.S. Mao, Titanium dioxide nanomaterials: synthesis, properties, modifications, and applications, Chem. Rev., 107 (2007) 2891–2959.
[6] T. Fotiou, T.M. Triantis, T. Kaloudis, A. Hiskia, Evaluation of the photocatalytic activity of TiO_2 based catalysts for the degradation and mineralization of cyanobacterial toxins and water off-odor compounds under UV-A, solar and visible light, Chem. Eng. J., 261 (2015) 17–26.
[7] M. Xing, Y. Zhou, C. Dong, L. Cai, L. Zeng, B. Shen, L. Pan, C. Dong, Y. Chai, J. Zhang, Y. Yin, Modulation of the reduction potential of TiO_{2-x} by fluorination for efficient and selective CH_4 generation from CO_2 photoreduction, Nano Lett., 18 (2018) 3384–3390.
[8] C. Dong, C. Lian, S. Hu, Z. Deng, J. Gong, M. Li, H. Liu, M. Xing, J. Zhang, Size-dependent activity and selectivity of carbon dioxide photocatalytic reduction over platinum nanoparticles, Nat. Commun., 9 (2018) 1252.
[9] S.F. Chen, J.P. Li, K. Qian, W.P. Xu, Y. Lu, W.X. Huang, S.H. Yu, Large scale photochemical synthesis of M@TiO_2 nanocomposites (M = Ag, Pd, Au, Pt) and their optical properties, CO oxidation performance, and antibacterial effect, Nano. Res., 3 (2010) 244–255.
[10] Z. Zheng, B. Huang, X. Qin, X. Zhang, Y. Daib and M-H. Whangbo, Facile in situ synthesis of visible-light plasmonic photocatalysts M@TiO_2 (M = Au, Pt, Ag) and evaluation of their photocatalytic oxidation of benzene to phenol, J. Mater. Chem., 21 (2011) 9079–9087.
[11] M. Maicu, M.C. Hidalgo, G. Colón, J.A. Navío, Comparative study of the photodeposition of Pt, Au and Pd on pre-sulphated TiO_2 for the photocatalytic decomposition of phenol, J. Photochem. Photobiol., A., 217 (2011) 275–283.
[12] F.J. Beltrán, F.J. Rivas, R. Montero-de-Espinosa, Comparative study of the photodeposition of Pt, Au and Pd on pre-sulphated TiO_2 for the photocatalytic decomposition of phenol, Appl. Catal., B., 39 (2002) 221–231.
[13] J. Marugán, R. Grieken, A.E. Cassano, O.M. Alfano, Scaling-up of slurry reactors for the photocatalytic oxidation of cyanide with TiO_2 and silica-supported TiO_2 suspensions, Catal. Today, 144 (2009) 87–93.
[14] S. Pakdaman, A. Ebrahimian, N. Gilani, Deposition of Ag nanoparticles onto TiO_2/Fe_3O_4/MWCNTs quaternary nanocomposite: a visible-light-driven plasmonic photocatalyst for degradation of 2,4-dichlorophenol, Desal. Wat. Treat., 102 (2018) 241–252.
[15] A. Gharaee, A. Ebrahimian, Z. Khodaee, Photodeposition of silver on p-Cu_2O/n-TiO_2 nanocomposite applied to visible light degradation of 2,4-dichlorophenol in synthetic wastewater, Desal. Wat. Treat., 114 (2018) 205–220.
[16] N. Esmaeili, A. Ebrahimian, Z. Khodaee, Visible-light active and magnetically recyclable Ag-coated Fe_3O_4 /TiO_2 nanocomposites for efcient photocatalytic oxidation of 2,4-dichlorophenol, Desal. Wat. Treat., 114 (2018) 251–264.
[17] A. Ebrahimian, P. Monazzam, B.F. Kisomi, Co/TiO_2 nanoparticles: preparation, characterization and its application for photocatalytic degradation of methylene blue, Desal. Wat. Treat., 63 (2017) 283–292.
[18] M. Iwasaki, M. Hara, H. Kawada, H. Tada, S. Ito, Cobalt ion-doped TiO_2 photocatalyst response to visible light, J. Colloid Interface Sci., 224 (2000) 202–204.

[19] S. Laurent, D. Forge, M. Port, A. Roch, C. Robic, L.V. Elst, R.N. Muller, Magnetic iron oxide nanoparticles: synthesis, stabilization, vectorization, physicochemical characterizations, and biological applications, Chem. Rev., 108 (2008) 2064–2110.
[20] J. Fu, Sh. Cao, J. Yu, Dual Z-scheme charge transfer in TiO_2/Ag/Cu_2O composite for enhanced photocatalytic hydrogen generation, J. Materiomics, 1 (2015) 124–133.
[21] Z. Mo, C. Zhang, R. Guo, S. Meng, J. Zhang, Synthesis of Fe_3O_4 nanoparticles using controlled ammonia vapor diffusion under ultrasonic irradiation, Ind. Eng. Chem. Res., 50 (2011) 3534–3539.
[22] J. Lu, M. Wang, C. Deng, X. Zhang, Facile synthesis of Fe_3O_4@ mesoporous TiO_2 microspheres for selective enrichment of phosphopeptides for phosphoproteomics analysis, Talanta, 105 (2013) 20–27.
[23] V.G. Deshmane, S.L. Owen, R.Y. Abrokwah, D. Kuilaa, Mesoporous nanocrystalline TiO_2 supported metal (Cu, Co, Ni, Pd, Zn, and Sn) catalysts: effect of metal-support interactions on steam reforming of methanol, J. Mol. Catal. A: Chem., 408 (2015) 202–213.
[24] Q. Chen, F. Ji, T. Liu, P. Yan, W. Guan, X. Xu, Synergistic effect of bifunctional Co–TiO_2 catalyst on degradation of Rhodamine B: fenton-photo hybrid process, Chem. Eng. J., 229 (2013) 57–65.
[25] M. Khan, W. Cao, Cationic (V, Y)-codoped TiO_2 with enhanced visible light induced photocatalytic activity: a combined experimental and theoretical study, J. Appl. Phys., 114 (2013) 183514.
[26] M. Hamadanian, A. Reisi-Vanani, A. Majedi, Sol-gel preparation and characterization of Co/TiO_2 nanoparticles: application to the degradation of methyl orange, J. Iran. Chem. Soc., 7 (2010) 52–58.
[27] I. Ganesh, A.K. Gupta, P.P. Kumar, P.S. Chandra Sekhar, K. Radha, G. Padmanabham, G. Sundararajan, Preparation and characterization of Co-doped TiO_2 materials for solar light induced current and photocatalytic applications, Mater. Chem. Phys., 135 (2012) 220–234.
[28] S. Kumar, S. Khanchandani, M. Thirumal, A.K. Ganguli, Achieving enhanced visible-light-driven photocatalysis using type-II $NaNbO_3$/CdS core/shell heterostructures, ACS Appl. Mater. Interfaces., 6 (2014) 13221–13233.
[29] S. Rehman, R. Ullah, A.M. Butt, N.D. Gohar, Strategies of making TiO_2 and ZnO visible light active, J. Hazard. Mater., 170 (2009) 560–569.
[30] O. Carp, C.L. Huisman, A. Reller, Photoinduced reactivity of titanium dioxide, Prog. Solid State Chem., 32 (2004) 33–177.
[31] N. Venkatachalam, M. Palanichamy, B. Arabindoo, V. Murugesan, Enhanced photocatalytic degradation of 4-chlorophenol by Zr^{4+} doped nano TiO_2, J. Mol. Catal. A: Chem., 266 (2007) 158–165.
[32] K.S.W. Sing, Reporting physisorption data for gas/solid systems with special reference to the determination of surface area and porosity (Recommendations 1984), Pure Appl. Chem., 57 (1985) 603–619.
[33] Z. Teng, X. Su, G. Chen, C. Tian, H. Li, L. Ai, G. Lu, Superparamagnetic high-magnetization composite microspheres with Fe_3O_4@SiO_2 core and highly crystallized mesoporous TiO2 shell, Colloids Surf., A., 402 (2012) 60–65.
[34] S.J. Yeo, H. Kang, Y.H. Kim, S. Han, P.J. Yoo, Layer-by-layer assembly of polyelectrolyte multilayers in three-dimensional inverse opal structured templates, ACS Appl. Mater. Interfaces., 4 (2012) 2107–2115.
[35] M. Asiltürk, F. Sayılkan, E. Arpaç, Effect of Fe^{3+} ion doping to TiO_2 on the photocatalytic degradation of Malachite Green dye under UV and vis-irradiation, J. Photochem. Photobiol., A., 203 (2009) 64–71.
[36] L. Wu, A. Li, G. Gao, Zh. Fei, Sh. Xu, Q. Zhang, Efficient photodegradation of 2,4-dichlorophenol in aqueous solution catalyzed by polydivinylbenzene-supported zinc phthalocyanine, J. Mol. Catal. A: Chem., 269 (2007) 183–189.